



# Thermal-Hydraulic Design Concept of the Solid-Target System of Spallation Neutron Source

F.Tanaka, T. Hibiki, Y. Saito, T. Takeda, K. Mishima\*

*Research Reactor Institute, Kyoto University, Kumatori, Sennan, Osaka 590-0494, Japan*

## 1. Introduction

Recently, several projects of constructing a pulsed spallation neutron source are being promoted around the world. A spallation neutron source is an essential research facility for fields of material science, life science and fundamental physics. At present the spallation neutron source being operated at the highest proton beam power (160kW; 750MeV-200 $\mu$ A) in the world is the ISIS spallation neutron source at the Rutherford Appleton Laboratory, United Kingdom. In Japan, the Japan Hadron Facility (JHF) at High Energy Accelerator Research Organization (KEK) has been proposed. The project is now combined with the neutron science project of the Japan Atomic Energy Research Institute (JAERI). In this project, a spallation neutron source with a liquid metal target is considered as a main facility and the spallation source with a solid target is considered as a back-up of the liquid metal target. Schematic of the proposed solid target is shown in Fig.1. In the initial project the spallation neutron source with solid heavy metal target was considered to be operated at 0.6MW proton beam power. The maximum heat density is estimated to be as high as 1000MW/m<sup>3</sup> at 0.6MW proton beam power. So the heat removal from the solid target can be a vital problem. For the thermal hydraulic design of the solid target, study on flow distribution in the coolant channels, heat transfer coefficient on the heated surface and critical heat flux (CHF) which defines the limit of heat removal is indispensable. The main aspect of the coolant channels is that the channel gap is very narrow (1-2mm) and the heated length is so short that the entrance effect may not be neglected. From this point of view, heat transfer experiments were performed in this study to collect experimental data systematically on heat transfer coefficient and critical heat flux for vertical upward and horizontal flows in a thin

---

\*The author to whom all correspondence should be addressed. Phone: +81 724 51 2449, Fax: +81 724 51 2637, email: mishima@rri.kyoto-u.ac.jp

rectangular channel simulating a coolant channel of the proposed spallation neutron source. Thermal-hydraulic correlations which can be used for design calculations were proposed based on the obtained data.

## 2. Thermal-Hydraulic Design Criteria

The following criteria are imposed on the thermal-hydraulic design of the solid target and cooling system.

- (1) Generally coolant boiling causes flow instability in the parallel channels, and has undesirable effects on the solid (the target and the beam window) surface and maybe on neutronics. For this, no boiling should be allowed in the target coolant channels under normal operating conditions, therefore:

$$T_w < T_{\text{ONB}}$$

- (2) To maintain the integrity of the solid target and beam window, the temperatures in the solid, i.e. the target and the beam window, should be below the maximum permissible temperature of the material at anytime and anywhere, so that

$$T_{\text{solid}} < T_{\text{max}}$$

The value of  $T_{\text{max}}$  should be determined taking account of the melting temperature, the effects of temperature on mechanical strength, etc. Temporarily,  $T_{\text{max}}$  is set at 573K.

- (3) If the boiling crisis occurs on the solid surface, the solid temperature may rise beyond the maximum permissible temperature of the material. Therefore, the critical heat flux for the occurrence of boiling crisis should not be reached under normal and abnormal operating conditions:

$$q_w < q_{\text{CHF}} / (\text{safety margin}).$$

Note that under some special conditions, no sharp increase of solid temperature is observed even if CHF is reached. If this happens in the solid target cooling, this criterion can be ignored.

- (4) The coolant flow should not cause any significant vibration, deformation, erosion of the solids, therefore:

$$v < v_{\text{crit}}$$

Where  $v_{\text{crit}}$  denotes the critical velocity to initiate significant vibration which may cause deformation or damage of the solid target. The critical velocity can be estimated to be, for example, one half of Miller's velocity.

- (5) Temperature gradient and transients in the solid should not cause excessive thermal stress, thermal shock and fatigue during the lifetime of the material, therefore:

$$\sigma_{\text{solid}} < \sigma_{\text{max}}$$

Where  $\sigma_{\text{solid}}$  and  $\sigma_{\text{max}}$  denotes the stress in the solid and maximum permissible stress for the solid material, relatively.

- (6) In addition, all the above criteria should be met even under the influence of radiation damage, radioisotope production and chemical reaction throughout the lifetime of the solid material. Therefore, care should be taken for the effects of swelling of the target and beam window, accumulation of  $^7\text{Be}$  and  $^3\text{H}$  in the solid and cooling system, as well as hydrogenation and embrittlement of the material.

### 3. Experiment

#### 3.1 Test sections and test loop

The test channels used in the experiment was a rectangular channel heated from both sides with gap thickness of 1.0mm and 1.5mm, channel width of 40mm and heated length of 98mm. The test channels were mounted vertically or horizontally for vertical upward flow or horizontal flow experiment, respectively. Fig.2 shows the cross sectional view of the both-side heated channel. The channel wall was consisted of a Teflon insulator and a nickel alloy (Inconel X-750) heater. A 30mm-wide and 1mm-thick Inconel X-750 plate was mounted flush with the Teflon insulator, so that 5mm-wide unheated zones were left on both sides of the heater to avoid the corner effect on CHF. The water flowed in the gap between the two walls, and the flow direction is shown with arrows in Fig.2.

The plate heater had a copper electrode at each end on which direct current electric voltage was applied, so that the heaters were joule-heated. Twenty two or twenty six alumel-chromel thermocouples were spot welded onto the back-side surface of the heater for vertical upward flow or horizontal flow experiment, respectively. Each thermocouple was lead through a tunnel in the Teflon insulator behind the heater to the outside of the test section and then connected to a burnout detector which actuated the switch to shut off the electric power supply to the test section when the temperature exceeds a preset value.

The schematic diagram of the test loop is shown in Fig.3. Purified water circulated in the loop and flowed through the channel upwardly to be heated and boiled in the heated section. Steam was separated from water in the vapor/liquid separator and was released into the atmosphere, thus the pressure at the exit of the heated section was kept near the atmospheric pressure. The water flow rate was measured with turbine

flow meters installed upstream of the pre-heater/cooler and the test section. The flow measurement error was estimated to be within 3%. The inlet water temperature was measured with a thermocouple installed just upstream of the heated section. The inlet water temperature was controlled by using the pre-heater/cooler to be 20, 40, and 60°C to study the effect of inlet water temperature on CHF. The deviation of the temperature was within  $\pm 3^\circ\text{C}$ .

### *3.2 Experimental procedure*

Critical heat flux was measured by increasing the heater power step by step, keeping the inlet water temperature and the inlet water flow rate at preset values. At each step, the heater power was held constant for a few minutes and the wall-temperature traces were observed. The procedure was repeated until any of the burnout detectors detect a sharp increase of the heater wall temperature due to CHF. Then the heater power was switched off at a preset value of the wall temperature to protect the heater. The preset value was determined after some trial to be an optimum value (250°C~400°C) depending upon the experimental condition. When a CHF was approached, the increment of the heater power was controlled within a few percent of the preceding value. The CHF was calculated from the values of the electric current and the voltage measured across the two electrodes at both end of the heater just before the initiation of the sharp increase in the wall temperature. The heat loss was estimated to be a few percent from the heat balance in the test section.

## **4. Results and discussions**

### *4.1 Heat transfer coefficient*

Fig.4 shows a typical result of the boiling curve in 1.5mm gap channel. Single phase and nucleate boiling heat transfer correlations are compared with the experimental results in the figure. The condition for ONB was determined as the condition where the HTC begins to rapidly increase from single-phase heat transfer.

The heat fluxes for onset of nucleate boiling predicted by Dittus-Boelter's and Thom's equations were in good agreement with the experimental data. Chen's equation reproduced overall tendency qualitatively in good agreement with the experimental data.

Fig.5 compares the experimental results with the Dittus-Boelter equation in the single-phase heat transfer region. Gnielinski's equation was used to estimate the entrance effect. Solid circles, triangles, and squares indicate vertical upward flow data

with inlet temperature 20, 40, and 60°C and the open symbols indicate horizontal flow data, respectively. Gnielinski's equation gave a fairly good prediction for the variation of Nusselt number with the distance from the inlet for both channel gaps. Similar results were also obtained for vertical upward flow and horizontal flow. This implies that no significant difference of the heat transfer mechanism exists between vertical upward and horizontal flows.

#### 4.2 Critical heat flux

Fig.6 compares the CHF of vertical upward flow with that of horizontal flow in different gap thickness. In the positive quality region, the CHF of vertical upward flow was higher than that of horizontal flow. The reason may be explained as follows. The burnout in the vertical upward flow occurs at the downstream of the test section in the region ( $G \leq 300 \text{ kg/m}^2\text{s}$ ) where the burnout is caused by the dry-out of liquid film on the heated wall. In the horizontal flow, generated steam tends to gather to the upper part of the flow channel due to the buoyancy force. In this situation, subcooled water may not be supplied sufficiently to the upper part filled with steam, resulting in the burnout there. This contributes to the decrease in the CHF in the horizontal flow. On the other hand, no significant difference of CHF between vertical upward and horizontal flows was found in the subcooled region. This implies that the burnout in the subcooled region both in the horizontal flow and the vertical upward flow occurs due to the same mechanism, namely DNB-type burnout. Figure 7 also shows the comparison of existing correlations discussed in Sec.2.2 with measured CHF. Modified-Thorgerson's equation gave the best prediction over the range of mass flux tested in this experiment. Sudo's equation gave about 30% conservative prediction in the quality region, though in the subcooled region the correlation tend to deviate from the data at high mass flux. Bernath's equation can be used for conservative estimation for the subcooled region.

### 5. Feasibility study on maximum power with solid target

The calculations were performed with the following conditions

- (1) The heat transfer coefficient for single-phase flow was calculated by the Dittus-Boelter correlation.
- (2) The heat transfer coefficient for boiling region was calculated by Chen's correlation.
- (3) Condition for the onset of nucleate boiling was calculated by the intersect between Thom's correlation and Dittus-Boelter correlation.
- (4) CHF was calculated by the modified Thorgerson's correlation.

- (5) The bulk coolant temperature was calculated by the half of the total heat generation per one target plate at the peak power density, but the coolant channel received the heat from both of the target plates adjacent to the channel and the target temperature was calculated with this bulk temperature and the peak power density obtained from Fig.6.

The results of the calculation are shown in Fig.7. Temperature variation of the target at location of peak heat flux is shown with beam power. Conditions of the target were calculated as follows: the coolant gap is 1.5mm, coolant velocity 10m/s, system pressure 0.1MPa, inlet temperature 30°C, length and thickness of the target plate was 170mm and 5mm respectively. From Fig.7, it can be seen that the most severe condition to limit the beam power is ONB and the beam power at the condition is 1.7MW. However, it should be noted that this calculation does not take account of the safety margin. In the thermal hydraulic design some safety margin should be taken account of. The safety margin should be determined based on the power peak factor, fabrication tolerance of the target and coolant channels, and some other engineering factors.

## 6. Summary

In relation to thermal-hydraulic design of the N-Arena solid-target system of the JHF project, heat transfer experiments were performed to obtain experimental data systematically on heat transfer coefficient and CHF for vertical upward and horizontal flows in a thin rectangular channel simulating a coolant channel of the proposed spallation neutron source. Thermal-hydraulic correlations which can be used for design calculations were proposed based on the obtained data. Finally tentative results of feasibility study on maximum beam power which could be attained with a solid target were presented. The result indicated that the condition for the onset of nucleate boiling is the most significant limiting factor to the maximum beam power.

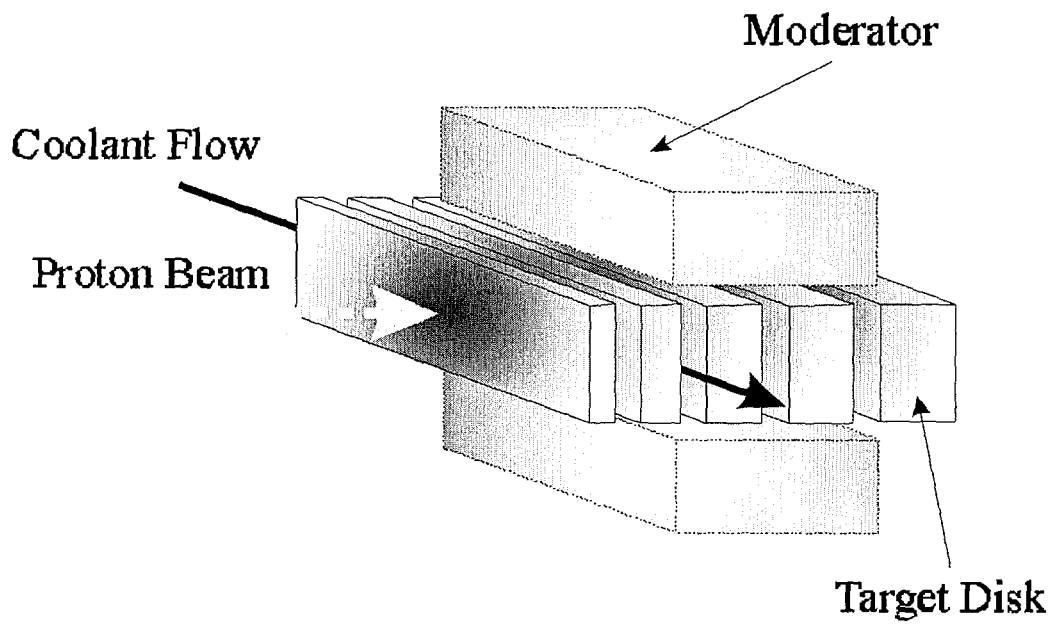


Fig.1 Schematic of the solid target

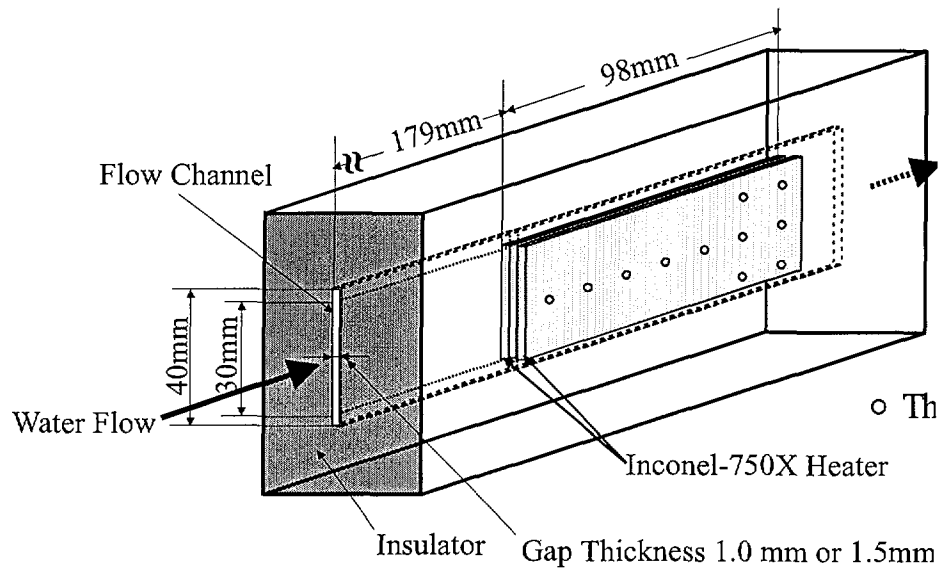


Fig.2 Cross sectional view of the test section

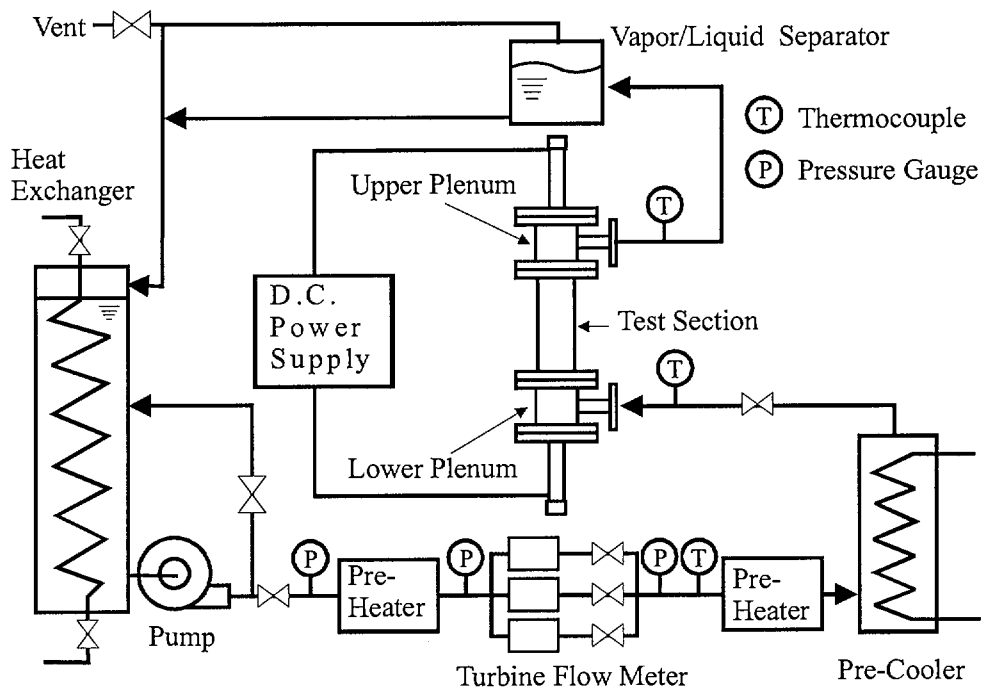


Fig.3 Schematic of the test loop

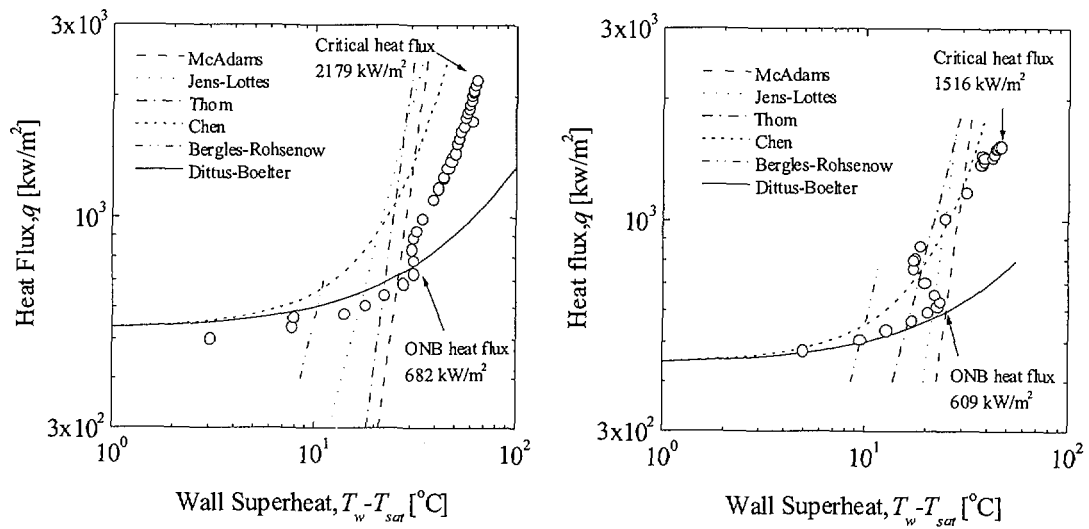


Fig.4 Typical result of boiling curve

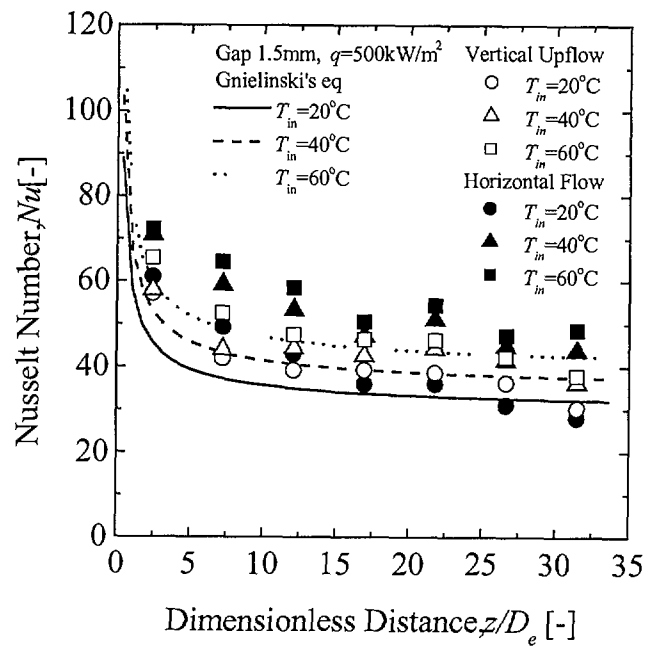


Fig.5 Variation of local Nusselt number with dimensionless distance

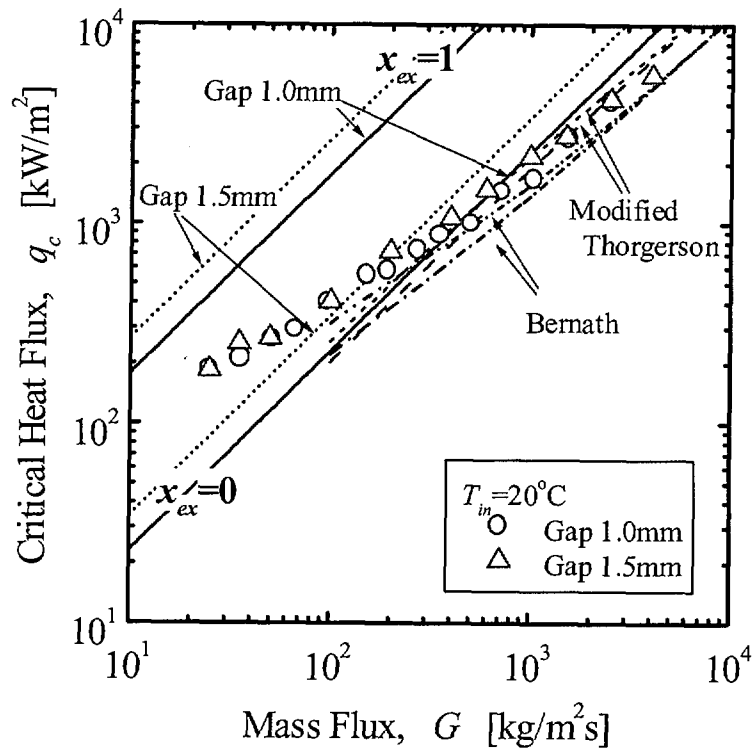


Fig.6 Variation of CHF with mass flux

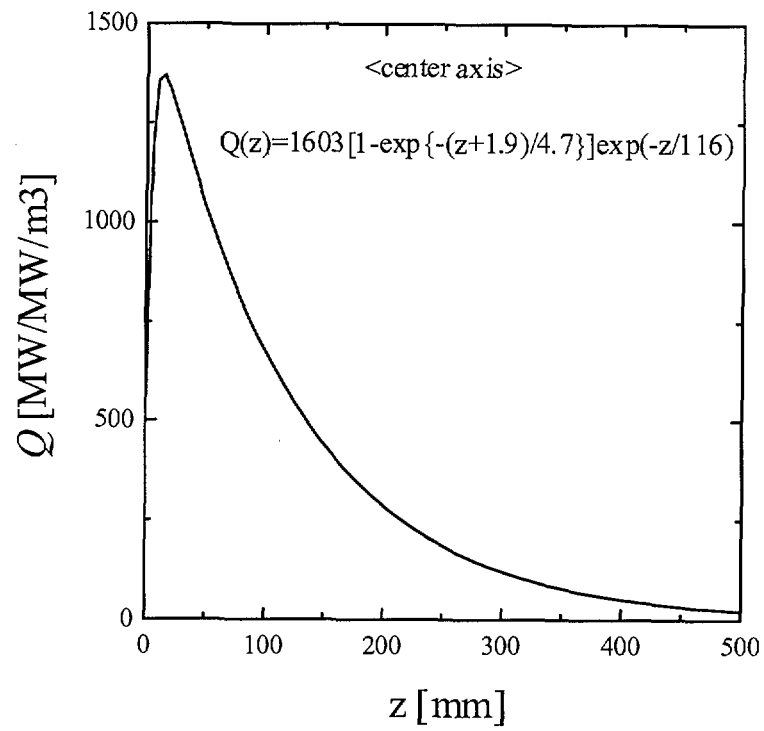


Fig.7 Heat generation density per beam power along the center axis of the target

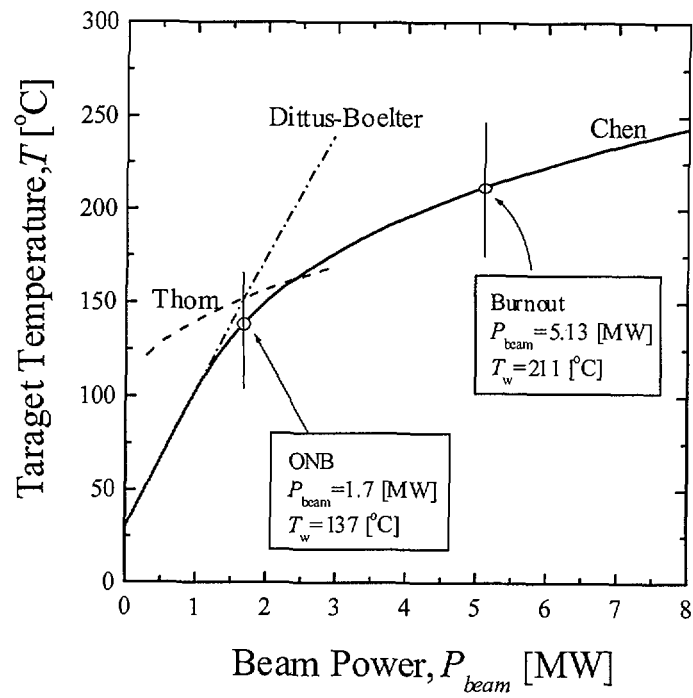


Fig.8 Temperature variation of solid target with beam power